Desalination and Water Treatment
www.deswater.com
doi: 10.1080/19443994.2015.1077743

57 (2016) 16300–16309
July

Taylor & Francis
Taylor & Francis Group

Chemical and electrochemical study of the inhibition of calcium carbonate precipitation using citric acid and sodium citrate

Amina Karar*, Farid Naamoune, Abdelkrim Kahoul

Laboratoire d'Energétique et d'Electrochimie des solides, Université F. Abbas de Sétif, Sétif 19000, Algérie, Tel. +213 6 64 02 47 53; emails: amina.karar@hotmail.fr (A. Karar), fnamoune@yahoo.fr (F. Naamoune), kahoulabdelkrim@yahoo.fr (A. Kahoul)

Received 7 November 2014; Accepted 25 July 2015

ABSTRACT

This work investigated the inhibitive effect of citric acid (CA), sodium citrate (SC), and their mixture (CA–SC) on the $CaCO_3$ scale. The study was carried out using chronoamperometry, impedancemetry, and fast-controlled precipitation methods. The electrochemical study showed that CA provides a slight inhibition of $CaCO_3$ deposit at a concentration of 70 ppm on stainless steel surface. The use of SC alone inhibits very little the formation of scale. The use of the mixture (50% of CA and 50% of SC) with small concentration led to significant inhibition of the $CaCO_3$ formation. The deposits formed were characterized by scanning electron microscope (SEM) and X-ray diffraction (XRD). The XRD showed that the intensity of the preferential orientation (1 0 4) corresponding to crystallographic plans of calcite decreases and the SEM demonstrated a decrease in calcite crystal size from 10 to about 2 μm.

Keywords: Calcium carbonate deposit; Inhibitor; Citric acid; Sodium citrate

1. Introduction

The precipitation of an insulating layer of scaling on the walls of the water distribution pipes has serious technical and economic consequences. Formation of insoluble mineral salts, such as calcium carbonate or barium sulfate, causes important problems in the industrial processes [1,2]. Various methods were used to prevent the scale formation in water [3] such as the chemical methods in which the germination of the $CaCO_3$ crystals is blocked using the inhibitor [4–6] and electrochemical methods using the chronoamperometry [7,8], impedancemetry [9,10], and electrogravimetry [11].

In recent years, a few studies have been focused on the aspects of the surface scaling so that the different mechanisms were proposed to explain the differences between the scaling precipitation in bulk solution and scale deposition at the surface. Klaren et al. [12] and Helalizadeh et al. [13] studied the scale formation of calcium carbonate and sulfate on the surface by monitoring the heat transfer properties through the scale deposition. Thus, a relative estimation of the scale thickness is estimated [14]. Morizot et al. [15] proposed a novel method to investigate scale deposition at the metal surfaces using an electrochemical technique with a rotating disk electrode.

Inhibitors commonly used in the industry include phosphonates, polyphosphonates, polyacrylates, and various other polymers [6]. The efficiency of phosphorous and nitrogen compounds for scale formation has already been demonstrated [16,17]. However, the use of such compounds generates a modification of the

*Corresponding author.

biological cycle. As reported by Camargo and Alonso [18], inhibitors are toxic to the environment and the health. In the case of the bacterial flora, they can act as disturbers of the ecosystem. One can cite the case of eutrophication, one of the most dramatic consequences is the deoxygenation of water that leads to the death of aquatic organisms. A number of antiscalants are commercially available and new formulations are continuously being developed and tested for calcium carbonate scaling such as gelatin, carboxymethyl cellulose, and keratin [19]. Abdel-Gaber et al. investigated Fig [20], and olive [21] leaves extracts. Abd-El-Khalek et al. [22] investigated palm leaves as novel environmentally friendly antiscalants. Chaussemier et al. [23] focused on some green antiscalants derived from petrochemicals, and resumed the efforts done these last years to obtain green inhibitors, either using natural organic molecules or extracted from plants.

Citric acid (CA) (2-hydroxy-1,2,3-propanetricarboxylic acid, $C_6H_8O_7$) is one of the most important organic acids used massively worldwide because of its low toxicity compared with other acidilants [24]. It can be used as an additive to add an acidic taste to food and soft drinks, and also as an ingredient in detergents and cleaning products [25]. Westin and Rasmuson [26] studied the behavior of calcium carbonate in the presence of CA. Using chemical speciation calculations, the actual thermodynamic driving force was determined. With increasing additive concentration the nucleation time and the interfacial energy increase. CA has the strongest effect on both nucleation time and on the estimated interfacial energy. They also studied [17] the crystal growth of aragonite and calcite in presence of CA at pH 8.5 by the constant supersaturation method. They demonstrated that CA affects the process of crystallization and growth of aragonite more than those of calcite. In their work, Wada et al. [27] coupled the pH-drift method and the light-scattering technique to study the influence of five natural carboxylic acids, namely malonic acid, maleic acid, succinic acid, tartaric acid, and CA, on $CaCO_3$ crystallization.

In the case of CA, a concentration of 13 mg/L appeared to be quite effective with a total calcium concentration of 800 mg/L. Calcium carbonate growth seemed to be inhibited by the adsorption of the carboxylic acid onto the $CaCO_3$ surface. Reddy et al. used the constant composition technique to determine the calcite growth rate in the presence of CA at 25°C and at pH 8.55 [28]. The authors showed that CA exhibited only moderate calcite crystal growth at concentrations as high as 10 mg/L. This could be related to the fact that CA is a linear polycarboxylic acid.

To the best of our knowledge, there is a lack of work concerning the use of CA and the mixture CA/citrate as inhibitors for $CaCO_3$ scale.

The aim of the present work is to study the inhibition of scaling by the mixture of CA and sodium citrate (SC). In order to evaluate the scale inhibitors' efficiency, electrochemical measurements (chronoamperometry and impedancemetry), together with scanning electron microscopy (SEM) and X-ray diffraction (XRD), were used for investigating the efficiency of mixture (CA–SC) on the inhibition of calcium carbonate deposition on a metallic surface. Fast controlled precipitation (FCP) tests were carried out in order to get some insight into scaling propensity of water.

2. Experimental

2.1. Materials

Bir Aissa groundwater supply for the city of Ras el Oued comes from limestone, and therefore it is supersaturated with calcium salts.

Analytical grade CA (2-hydroxy-1,2,3-propanetricarboxylic, $C_6H_8O_7{\cdot}2H_2O$) and hydrated SC (trisodium 2-hydroxypropane-1,2,3-tricarboxylate, $Na_3C_6H_5O_7{\cdot}2H_2O$) were obtained from Sigma-Aldrich chemical company. All chemicals are reagent grade and were used as received.

2.2. Electrochemical techniques

Chronoamperometry was the first technique in the analysis of the process of the scaling accelerated by electrochemical way. The application of a cathodic potential (−1,050 mV) [7,8] to the electrode leads to the formation of a deposit of carbonate of calcium. It is formed following a local increase in interfacial pH electrode/solution [29] by the following reaction:

$$O_2 + 2H_2O + 4e^- \longrightarrow OH^- \quad (1)$$

This increase in interfacial pH causes a displacement of the equilibrium of carbonates, thus, inducing the calcium carbonate formation [30,31]:

$$HCO_3^- + OH^- \longrightarrow CO_3^{2-} + H_2O \text{ (in bulk)} \quad (2)$$

$$Ca^{2+} + CO_3^{2-} \longrightarrow CaCO_3 \text{ (at the interface)} \quad (3)$$

The electrochemical study was carried out in a standard three-electrode electrolytic cell. The reference

was saturated calomel electrode (SCE). All potentials were given with reference to this electrode. The counter electrode was a platinum plate of 0.94 cm^2 area. The working electrode was a disk of stainless steel of 0.8 cm^2 area. The potentiodynamic measurements were carried out using VoltaLab PG301, which was controlled by Voltamaster4 software. The measurement of the electrochemical impedance of the metal-deposition interface of calcium carbonate allows the assessment of adherence character [32–34]. The electrochemical impedance spectroscopy (EIS) measurements were carried out using a transfer function analyzer (VoltaLab PG301), with a small amplitude ac. signal (10 mV), over a frequency domain from 100 kHz to 50 mHz, and an air atmosphere.

2.3. Fast controlled precipitation method (FCP)

According to Ledion et al. [35], in order to precisely characterize the scaling power of water, the principle of the test is to bring the degree of supersaturation between 20 and 30. To do this, agitation of solution by degassing CO_2 dissolved in water leads to an increase in pH due to the increase of OH^- ions formed. There is production of ions CO_3^{2-} which react with Ca^{2+} to form $CaCO_3$ [36]. 400 ml of raw water and 400 ml of treated water were introduced into two round similar bottom flasks and heated at a temperature of 40°C. These two solutions were stirred at 800 rpm. After every 5 min, the pH and resistivity values were measured using a pH meter (INOLAB pH 7310) and multiparameter (Multi 3420 wtw), respectively.

2.4. Instrumentation

XRD measurements were conducted using a Philips X-Pert diffractometer with Cu Kα radiation (1.5406 Å). The surface morphology of films was investigated by a JSM-7001F scanning electron microscope (SEM). The elemental composition was obtained using energy-dispersive X-ray spectrometer (EDS) connected to the SEM.

3. Results and discussions

3.1. Chemical study

All the physicochemical parameters of the studied water are shown in Table S1. It should be noted that the Bir Aissa water is naturally rich in minerals. Moreover, it contains calcium and magnesium. Therefore, it has a high hardness.

The composition of the scale formed chemically is confirmed by XRD and IR, which is essentially a mixture of three polymorphisms of $CaCO_3$: vaterite, calcite, and aragonite. The composition of scale is summarized in Fig. S1.

3.2. Study of inhibition by CA

The inset in Fig. 1(a) shows a chronoamperogram for Bir Aissa raw water. When the potential is applied, the system needs a few seconds to reach dynamic

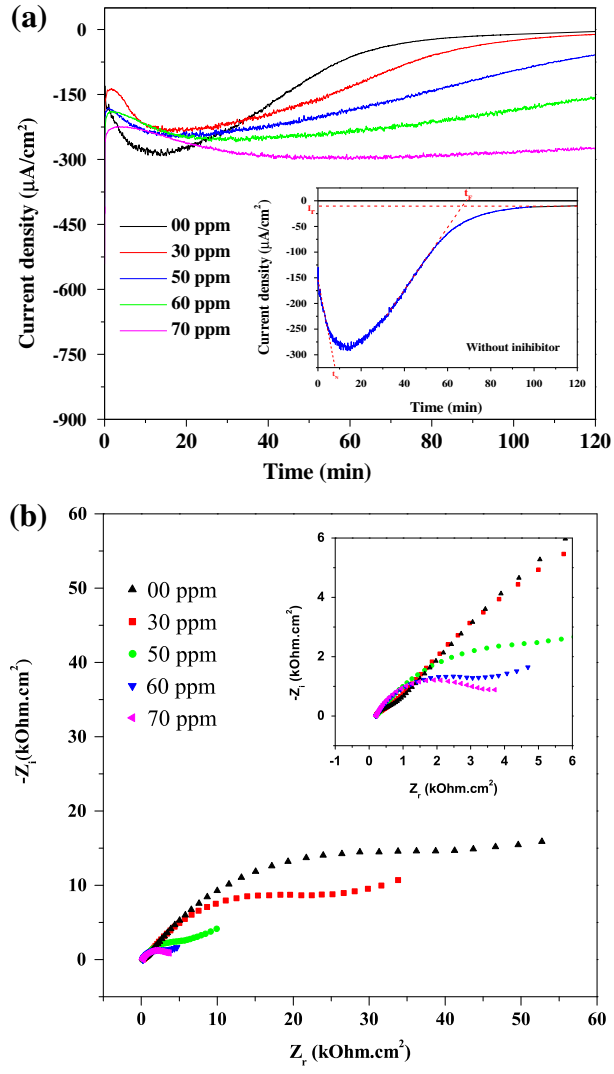

Fig. 1. (a) Chronoamperograms for polarized stainless steel electrode at E = −1,050 mV/SCE, (rotation speed = 400 rpm) in Bir Aissa water in the absence and presence of different concentrations of CA and (b) impedance spectra at open circuit of stainless steel in the same water in the absence and presence of different concentrations of CA.

Table 1
Characteristic parameters obtained from the chronoamperomgrams

Concentration CA	00 ppm	30 ppm	50 ppm	60 ppm	70 ppm
Germination time (min)	7.97	29.33	38.67	74.03	107.41
Nucleation time (min)	70.03	91.41	140.46	226.07	–
Residual current (μA/cm^2)	6.13	14.82	71.86	168.45	275.96

equilibrium to allow the formation of the layer of diffusion; this one is related to the reduction of dissolved oxygen, when the current density increases at the beginning of the curve. The result shows that after 120 min immersion time of electrode in the scaling solution a double layer of crystal might be formed at the same part of the metal surface [37].

It is noted that the current density decreases rapidly because the formation of OH^- ions, by reducing, causes alkalinity of the electrode/solution interface. This leads to formation of a $CaCO_3$ deposit according to Eq. (2). The current density continues to decrease until a residual current (i_r) value of 6 μA/cm is obtained after 120 min of deposition. Thus, the diffusion of O_2 is partially or totally blocked by the deposit formed on the electrode surface.

The chronoamperograms for various concentrations of CA (30, 50, 60, and 70 ppm) are shown in Fig. 1(a). The results collected in Table 1 from the curves indicate that in absence of the inhibitor, the nucleation time (t_n) is short and the residual current (i_r) is small. On the other hand, t_n and i_r increase with increasing the CA concentration to reach the value of 275 μA/cm^2. The kinetics of deposition is thus slowed down and its mechanism is modified.

To characterize the deposits generated on the surface, measurements of EIS were made at an open circuit after 120 min of polarization in the solution containing various concentrations of CA. Fig. 1(b) shows that, in absence of CA, the spectrum consists of two loops. According to Devos et al. [38], one loop at high frequency (HF) is due to activation (charge transfer process of oxygen and water) and, one, at low frequency (LF), due to convection (diffusion process of oxygen). It is noted that the size of the capacitive loop at HF decreases as compared to that of the electrode, obtained in the absence of inhibitor. Indeed, this decrease in loop size could be attributed to the inhibition of the formation of $CaCO_3$.

When the amount of CA increases from 50 to 70 ppm, the capacitive loop at LF disappears, indicating that the charge transfer process of oxygen and water is very fast on the bare surface of the steel.

To complete the study of CA as an antiscalant for high hardness water, we use the FCP method to evaluate the CA efficiency for homogeneous nucleation. Different concentrations (0, 10, 25, 30, 40, 50, and 70 ppm) are, therefore, added. Fig. 2 shows both the two series of curves, pH and resistivity (ρ) vs. time.

According to the pH curves, one can distinguish the pH_{limit} and t_{limit}. Indeed, pH_{limit} corresponds to the threshold of precipitation when the homogeneous

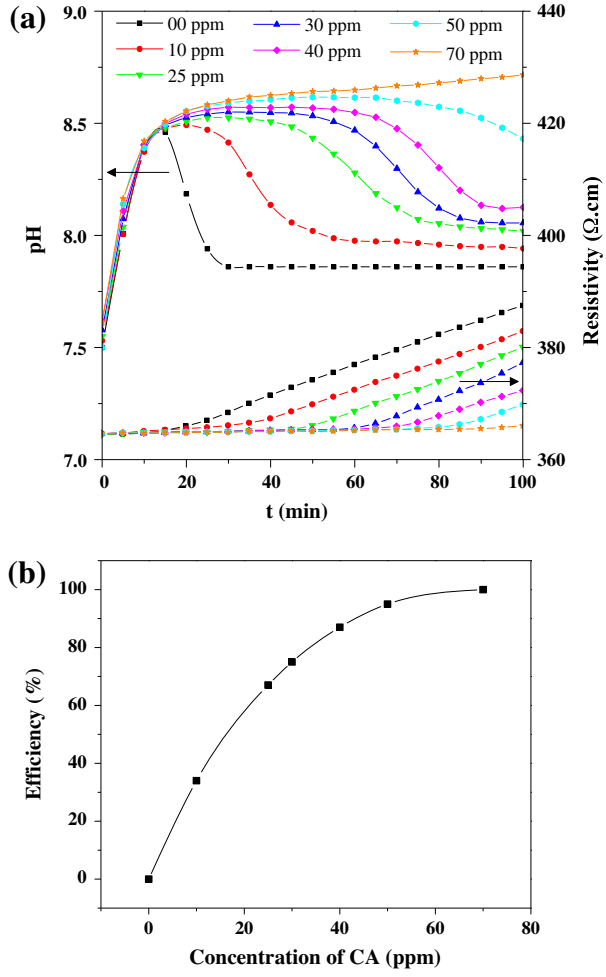

Fig. 2. (a) Variation of the pH and resistivity vs. time at 40°C for Bir Aissa water without and with varying concentrations of CA and (b) evolution of inhibition efficiency vs. concentration of CA.

Table 2
Evolution of pH_{limit} and t_{limit} vs. concentration of CA using FCP method

	00 ppm	10 ppm	25 ppm	30 ppm	41 ppm	50 ppm	70 ppm
pH_{limit}	7.9	8.05	8.31	8.39	8.42	8.68	–
t_{limit} (min)	15	40	60	70	75	90	–

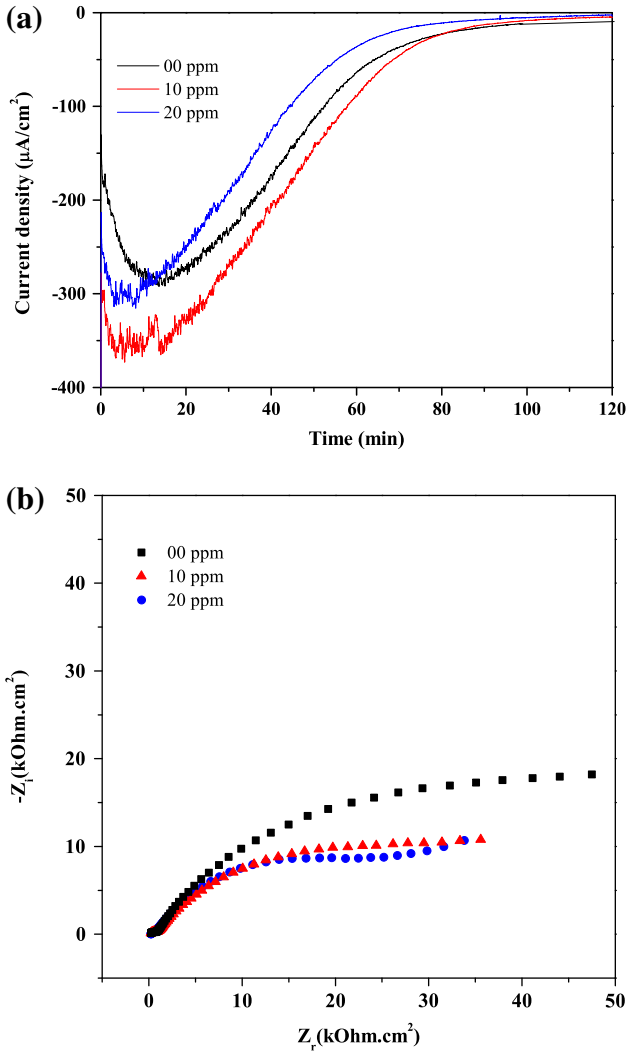

Fig. 3. (a) Chronoamperograms curves for polarized stainless steel electrode at $E = -1{,}050$ mV/SCE (rotation speed = 400 rpm) in Bir Aissa water in the absence and presence of different concentrations of SC and (b) impedance spectra at open circuit of stainless steel in the same water in the absence and presence of different concentrations of SC.

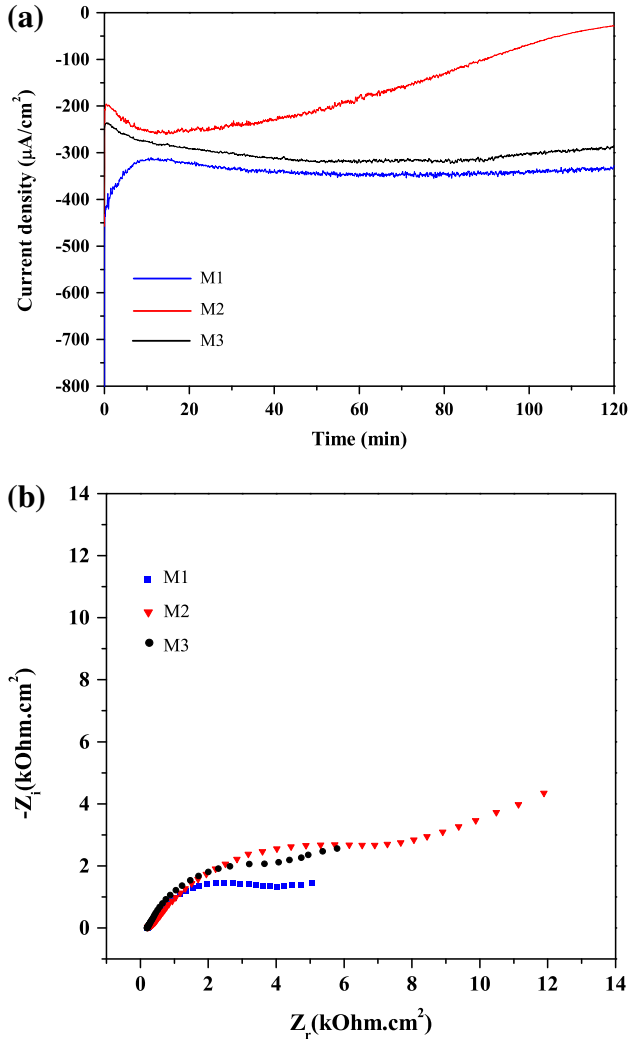

Fig. 4. (a) Chronoamperograms curves for polarized stainless steel electrode at $E = -1{,}050$ mV/ECS (rotation speed = 400 rpm) in Bir Aissa water in the presence of different concentrations of mixture (CA–SC) and (b) impedance spectra at open circuit of stainless steel in the same water in the presence of different concentrations of mixture (CA–SC).

precipitation occurs. The FCP experiments show two domains. The first one is seen for $t < t_{limit}$, and in which colloidal $CaCO_3$ nuclei appear. These nuclei can adhere strongly to the metal wall and promote the development of scale. The second domain reflecting a homogeneous precipitation in which $t > t_{limit}$, the

Table 3
Different percentages and pH of mixture (CA–SC) used

Mixture	CA (% mol.)	SC (% mol.)	pH
M1	50	50	7.4
M2	25	75	7.39
M3	75	25	7.45

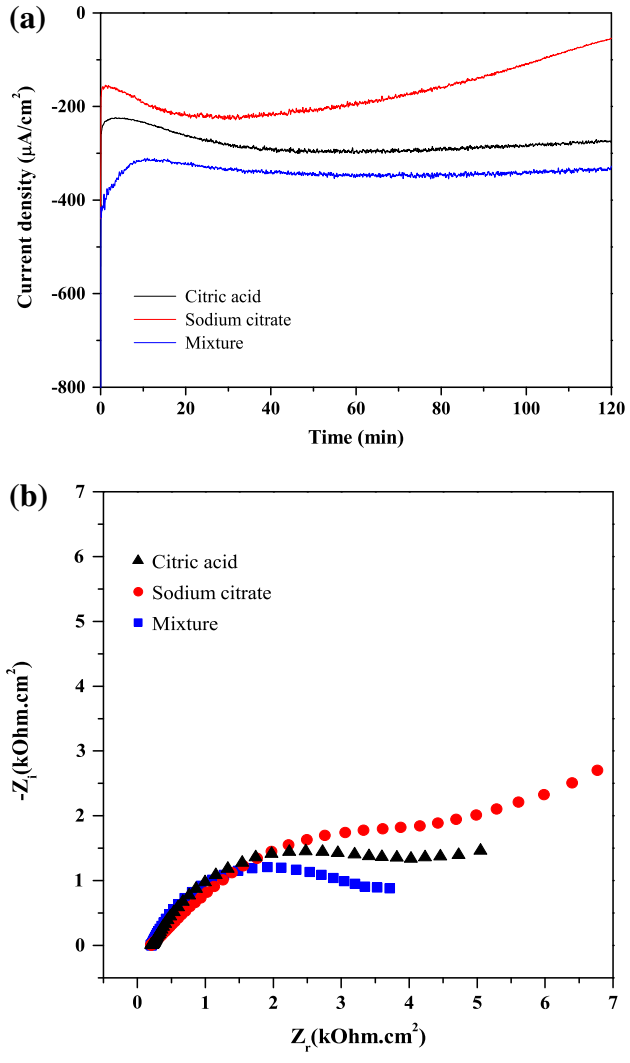

Fig. 5. (a) Chronoamperograms curves for polarized stainless steel electrode at $E = -1{,}050$ mV/ECS (rotation speed = 400 rpm) in Bir Aissa water in the presence of different inhibitors and (b) impedance spectra of stainless steel at open circuit in the same water in presence of different inhibitors.

nucleation is rapid, massive, and followed by a growth phase [39].

According to Table 2, it can be noted that, when the concentration of CA increases, both pH_{limit} and t_{limit} increase.

The efficiency of inhibition is determined by the following equation:

$$E = \frac{\int \rho_0 \times dt - \int \rho_i \times dt}{\int \rho_0 \times dt - \int \rho_{np} \times dt} \quad (4)$$

where ρ_0 is the resistivity of the raw water without CA, ρ_i is the resistivity of the raw water with CA, and ρ_{np} is the resistivity of the water which does not precipitate (raw water containing 70 mg/L of CA).

According to Eq. (4), efficiency as a function of concentration is shown in Fig. 2(b). It is also noted that the efficiency increases with increasing the concentration of CA. When the concentration reaches 70 ppm, the CA additive showed a total of inhibition efficiency.

3.3. Mixture of CA and SC

We demonstrated that CA provides a better inhibition efficiency in drilling water at a concentration 70 ppm, but the amount of inhibitor remains high enough in drinking water. On the other hand, the use of SC as inhibitor provides a too low inhibition efficiency according to chronoamperometry and impedance results shown in Fig. 3 and those of FCP shown in Fig. S2. It appears that the mixture of the two inhibitors has a synergic effect on preventing the scale deposition by chelating Ca^{2+} ions.

Fig. 4 presents cathodic curves and the impedance diagrams for the different concentrations of mixture (Table 3). It can be concluded from the chronoamperograms that the best mixture is M1, with a residual current of 334 µA/cm^2, reflecting a low $CaCO_3$ deposit on stainless steel electrode. The FCP measurments also carried out and the results are in good agreement with

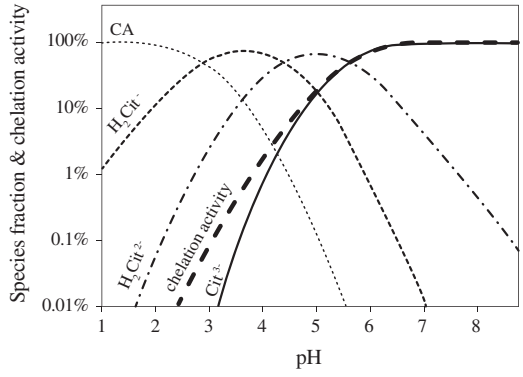

Fig. 6. Relationship between each form of CA (H_2Cit^-, $Hcit^{2-}$, Cit^{3-}) and their calcium chelation activity [41].

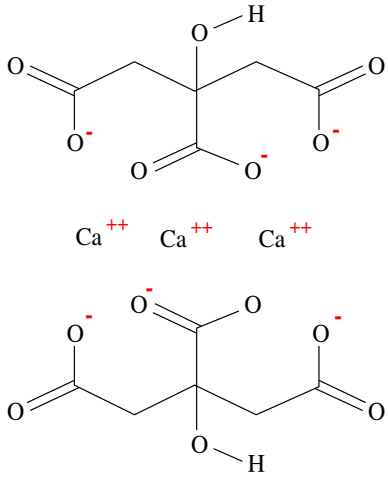

Fig. 7. Molecular structure of the complex CaCit.

those obtained by chronoamperometry on different mixtures (shown in Fig. S3).

The impedance diagram, corresponding to M1 gives a capacitive loop with the smallest diameter, reflecting low-scale deposit and surface coverage.

To better observe the mixture efficiency and to compare it with that of CA and SC, the chronoamperograms and impedance diagrams corresponding to the three inhibitors are presented in Fig. 5.

It can be seen that the mixture M1 inhibits strongly $CaCO_3$ deposit growth by delaying nucleation, compared to the two inhibitors less effective when used separately. The impedance diagram shows a loop with reduced diameter size, indicating inhibition of the scale formation.

The CA dissociates as follows:

$$H_3Cit \leftrightarrow H_2Cit^- + H^+ \quad pK_{a1} = 3.3$$

$$H_2Cit^- \leftrightarrow HCit^- + H^+ \quad pK_{a2} = 4.76$$

$$HCit^- \leftrightarrow Cit^{3-} + H^+ \quad pK_{a3} = 6.4$$

At pH values of mixture (Table 3), higher than pK_{a3}, the species Cit^{3-} predominates, leading to a complete chelation of Ca^{2+} cations, in good agreement with the

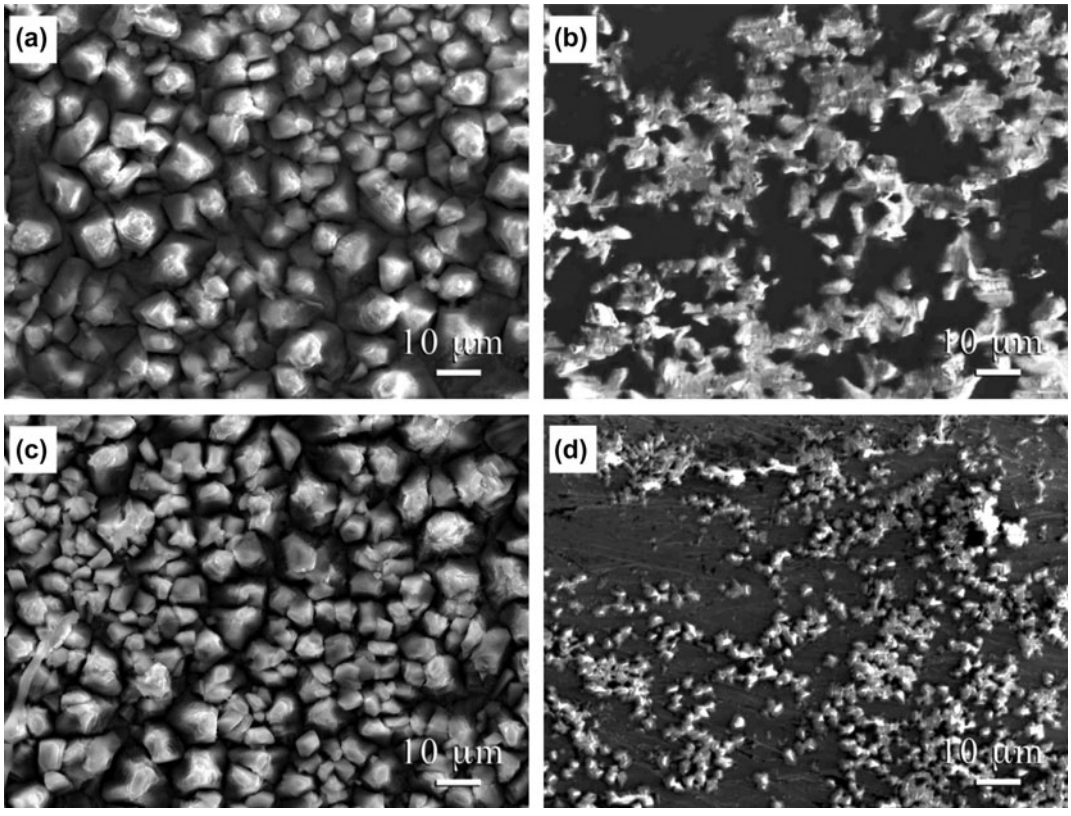

Fig. 8. Scanning electron microscopy of scale deposits obtained by electrodeposition after 120 min: (a) without inhibitor, (b) with 70 ppm of CA, (c) with 20 ppm of SC, and (d) with the mixture of CA and SC.

results of chelation acticity reported by Welling et al. [40] in Fig. 6.

In addition, the mixture (buffer solution) at pH 7.4 leads to formation of Cit^{3-} ions, resulting from deprotonation of CA in presence of SC, and citrate ions are chelated at calcium and form calcium–CA complexes; the formed calcium–CA complexes become calcium tetrahydrated citrate (CaCit; $Ca_3(C_6H_5O_7)_2{\cdot}4H_2O$) [41] as shown in Fig. 7.

To confirm results of $CaCO_3$ growth inhibition, a characterization of the deposits formed on the stainless steel electrode for different inhibitors is carried out.

3.4. Morphological and structural studies

The SEM microscopy was carried out for the various deposits formed in the absence and presence of inhibitors. The SEM micrographs in Fig. 8 show cubic crystals corresponding to the $CaCO_3$ calcite form [42,43]. It appears that the SC did not inhibit the calcite growth. In presence of mixture, fewer grains with small sizes are observed (from 10 to 2 μm).

To confirm the SEM observation, EDS analysis shows a sharp decrease in Ca^{2+} weight ration in presence of mixture (from 40 to 12.7 wt.%), in comparison with those of Ca^{2+} in presence of CA (20 wt.%) and SC (31.5 wt.%) additives.

In order to examine the microstructural evolution of the $CaCO_3$ deposits obtained in the absence and presence of different inhibitors, XRD measurements were performed on deposits obtained with CA, SC, and CA–SC after polarizing electrodes during 120 min (Fig. 9). All the peaks are in good agreement with those of the typical $CaCO_3$ diffraction pattern (JCPDS no. 00-047-1743), and no additional peaks corresponding to other phases are present.

It can be seen that the deposit of $CaCO_3$ shows a preferential orientation direction along the (1 0 4) direction detected at 29.72°, suggesting that the obtained grains correspond to crystallographic plans of calcite [9]. Another peak characteristic of calcite (0 1 8) at 2θ of 47.3° is observed. The comparison of spectra in Fig. 9 shows a decrease of the peak intensities of the calcite with the inhibitors used. In contrast to that obtained in presence of SC (Fig. 9(c)), the peak (1 0 4) intensity of calcite obtained in presence of CA (Fig. 9(d)) decreases strongly. Better results are obtained with the mixture as shown in Fig. 9(e), where a significant decrease is observed in intensity of the peak (1 0 4), and therefore an increase of calcite inhibition on the substrate.

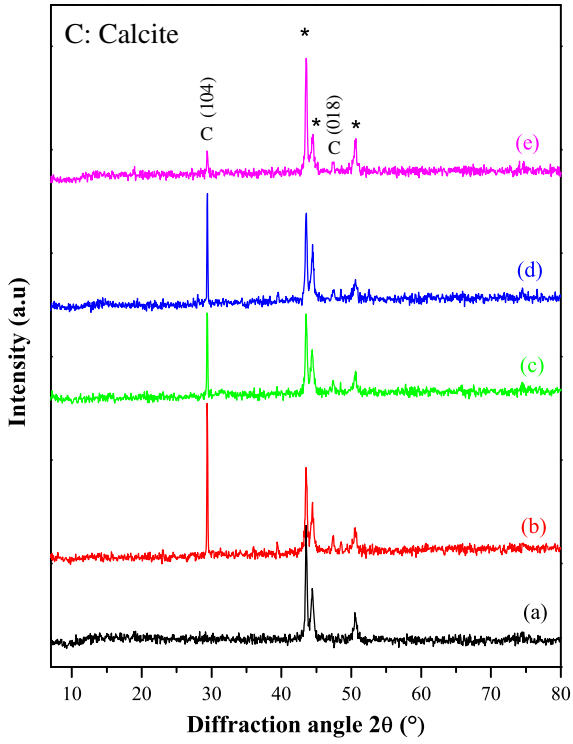

Fig. 9. XRD spectra of deposits: (a) stainless steel, (b) $CaCO_3$ deposited in absence of inhibitor, (c) $CaCO_3$ deposited in presence of SC, (d) $CaCO_3$ deposited in presence of CA, and (e) $CaCO_3$ deposited in presence of mixture. (*) indicates stainless steel peaks.

4. Conclusion

(1) $CaCO_3$ of Bir Aissa water (Algeria) formed chemically contains three polymorphs: calcite, aragonite, and vaterite, while $CaCO_3$ deposited electrochemically on stainless steel is essentially calcite;
(2) Chronoamperometry and impedance measurements showed that the optimal concentration of CA as inhibitor for calcite deposit is higher (70 ppm).
(3) Using SC, an incomplete inhibition of $CaCO_3$ deposit is observed.
(4) The use of the mixture of CA and SC showed better inhibition for $CaCO_3$ deposit with small concentrations. It appears that the mixture of the two inhibitors has a synergic effect on preventing the scale deposition by chelating Ca^{2+} ions. The nucleation time is increased and the growth crystal size is reduced.
(5) The FCP measurements carried out on different concentrations of mixture are in good agreement with those obtained by chronoamperometry on the same mixture.

Supplementary material

The supplementary material for this paper is available online at http://dx.doi.10.1080/19443994.2015.1077743.

Acknowledgment

This research was financially supported by University of Sétif-1-Algeria (Project J0101220100076).

Abbreviations

CA	—	citric acid
SC	—	sodium citrate
SEM	—	scanning electron microscope
XRD	—	X-ray diffraction
SCE	—	saturated calomel electrode
t_n	—	nucleation time
i_r	—	residual current
FCP	—	fast controlled precipitation
EIS	—	electrochemical impedance spectroscopy
HF	—	high frequency
LF	—	low frequency

References

[1] K.S. Sorbie, E.J. Mackay, Mixing of injected, connate and aquifer brines in waterflooding and its relevance to oilfield scaling, J. Pet. Sci. Eng. 27 (2000) 85–106.
[2] M. Crabtree, D. Eslinger, P. Fletcher, A. Johnson, G. King, Fighting scale-removal and prevention, Oilfield Rev. 11 (1999) 30–45.
[3] R. Rosset, M. Zidoune, C. Gabrielli, M. Keddam, G. Maurin, H. Perrot, Caractérisation du pouvoir incrustant d'une eau et évaluation de l'efficacité d'un traitement antitartre chimique au moyen d'une sonde thermique (Characterization of encrusting power of a water and assessing the efficiency of a chemical antiscalant treatment using a thermal sensor), Comptes rendus de l'Académie des sciences. Série II, Mécanique, Physique, Chimie, Astronomie 322 (1996) 335–341.
[4] H. Meyer, The influence of impurities on the growth rate of calcite, J. Cryst. Growth 66 (1984) 639–646.
[5] S. Ghizellaoui, M. Euvrard, Assessing the effect of zinc on the crystallization of calcium carbonate, Desalination 220 (2008) 394–402.
[6] J.M. Matty, M.B. Tomson, Effect of multiple precipitation inhibitors on calcium carbonate nucleation, Appl. Geochem. 3 (1988) 549–556.
[7] J. Ledion, P. Leroy, J.P. Labbe, Détermination du pouvoir incrustant d'une eau par un essai d'entartrage accéléré, (Determination of encrusting power of a water by accelerated scaling test) TSM-l'eau 80 (1985) 323–328.
[8] W. Lin, H. Karoui, B. Riffault, M. Jeannin, A. Kahoul, O. Gil, M. Ben Amor, M.M. Tlili, Mettre electrochemical scaling of stainless steel in artificial seawater: Role of experimental conditions on $CaCO_3$ and $Mg(OH)_2$ formation, Desalination 311(15) (2013) 234–240.
[9] C. Gabrielli, M. Keddam, A. Khalil, R. Rosset, M. Zidoune, Study of calcium carbonate scales by electrochemical impedance spectroscopy, Electrochim. Acta 42 (1997) 1207–1218.
[10] A. Khalil, C. Colin, C. Gabrielli, M. Keddam, R. Rosset, Caractérisation du pouvoir incrustant d'une eau et évaluation de l'efficacité d'un traitement antitartre chimique par impedancemétrie et microscopie électronique à balayage, (Characterization of power encrusting of a water and assessing the efficiency of a chemical anti-scaling treatment by impedance and scanning electron microscopy), Comptes Rendus de l'Académie des Sciences 316 (1993) 19–24.
[11] A. Khalil, P. Sassiat, C. Colin, C. Meignen, C. Garnier, C. Gabrielli, M. Keddam, R. Rosset, Caractérisation du pouvoir incrustant d'une eau par chronoélectrogravimétrie au moyen d'une microbalance à quartz, (Characterization of power encrusting of a water by chronoelectrogravimetry using a quartz microbalance) Comptes rendus de l'Académie des sciences 314 (1992) 145–149.
[12] D.G. Klaren, E.F. De Boer, D.W. Sullivan, "Zero fouling" self-cleaning heat exchanger, Heat Transfer. Eng. 28 (2007) 216–221.
[13] A. Helalizadeh, H. Muller-Steinhagen, M. Jamialahmadi, Crystallization fouling of mixed salts during convective heat transfer and sub-cooled flow boiling conditions, in: ECI Conference on Heat Exchanger Fouling and Cleaning: Fundamentals and Applications, USA, 2003.
[14] K. Peyvandi, A. Haghtalab, M.R. Omidkhah, Using an electrochemical technique to study the effective variables on morphology and deposition of $CaCO_3$ and $BaSO_4$ at the metal surface, J. Cryst. Growth 354 (2012) 109–118.
[15] A.P. Morizot, A. Neville, T. Hodgkiess, Electrochemical aspects of surface/solution interactions in scale initiation and growth, Mater. Perform. 37 (1998) 50–57.
[16] T. Chen, A. Neville, K. Sorbie, Z. Zhong, Using in situ synchrotron radiation wide angle X-ray scattering (WAXS) to study $CaCO_3$ scale formation at ambient and elevated temperature, Faraday Discuss. 136 (2007) 355–365.
[17] K.J. Westin, Å.C. Rasmuson, Crystal growth of aragonite and calcite in presence of citric acid, DTPA, EDTA and pyromellitic acid, J. Colloid Interface Sci. 282 (2005) 359–369.
[18] J.A. Camargo, Á. Alonso, Ecological and toxicological effects of inorganic nitrogen pollution in aquatic ecosystems: A global assessment, Environ. Int. 32 (2006) 831–849.
[19] E.R. McCartney, A.E. Alexander, The effect of additives upon the process of crystallization, J. Colloid Sci. 13 (1958) 383–396.
[20] A.M. Abdel-Gaber, B.A. Abd-El-Nabey, E. Khamis, D.E. Abd-El-Khalek, Investigation of fig leaf extract as a novel environmentally friendly antiscalent for $CaCO_3$ calcareous deposits, Desalination 230 (2008) 314–328.
[21] A.M. Abdel-Gaber, B.A. Abd-El-Nabey, E. Khamis, D.E. Abd-El-Khalek, A natural extract as scale and corrosion inhibitor for steel surface in brine solution, Desalination 278 (2011) 337–342.

[22] D.E. Abd-El-Khalek, B.A. Abd-El-Nabey, M.A. Abdel-kawi, S.R. Ramadan, Investigation of a novel environmentally friendly inhibitor for calcium carbonate scaling in cooling water, Desalin. Water Treat. (2014) 1–7.
[23] M. Chaussemier, E. Pourmohtasham, D. Gelus, N. Pécoul, H. Perrot, J. Lédion, H. Cheap-Charpentier, O. Horner, State of art of natural inhibitors of calcium carbonate scaling. A review article, Desalination 356 (2015) 47–55.
[24] A. Karthikeyan, N. Sivakumar, Citric acid production by Koji fermentation using banana peel as a novel substrate, Bioresour. Technol. 101 (2010) 5552–5556.
[25] J.L. Wu, Q.J. Peng, W. Arlt, M. Minceva, Model-based design of a pilot-scale simulated moving bed for purification of citric acid from fermentation broth, J. Chromatogr. A 1216 (2009) 8793–8805.
[26] K.J. Westin, Å.C. Rasmuson, Nucleation of calcium carbonate in presence of citric acid, DTPA, EDTA and pyromellitic acid, J. Colloid Interface Sci. 282 (2005) 370–379.
[27] N. Wada, K. Yamashita, T. Umegaki, Effects of carboxylic acids on calcite formation in the presence of Mg^{2+} ions, J. Colloid Interface Sci. 212 (1999) 357–364.
[28] M.M. Reddy, A.R. Hoch, Calcite crystal growth rate inhibition by polycarboxylic acids, J. Colloid Interface Sci. 235 (2001) 365–370.
[29] C. Deslouis, D. Festy, O. Gil, V. Maillot, S. Touzain, B. Tribollet, Characterization of calcareous deposits in artificial sea water by impedances techniques: 2-deposit of $Mg(OH)_2$ without $CaCO_3$, Electrochim. Acta 45 (2000) 1837–1845.
[30] L. Legrand, P. Leroy, Nouvelle méthode d'évaluation des procédés d'entartrage (New method of assessing scaling processes), Edition Eyrolles, Paris, 1981.
[31] D.M. Kern, The hydration of carbon dioxide, J. Chem. Educ. 37 (1960) 14–23.
[32] F. Hui, J. Lédion, Méthodes d'évaluation du pouvoir entartrant de l'eau (Evaluation Methods of power of the scaling water), J. Eur. Hydrol. 1 (2002) 1–27.
[33] C. Gabrielli, M. Keddam, G. Maurin, R. Perrot, R. H-Rosset, M. Zidoune, Caractérisation du pouvoir incrustant d'une eau par impedancemétrie, chrono électrométrie et microscopie électronique à balayage (Characterization of encrusting power of water by impedance, chronoelectrometry and scanning electron microscopy), in: Eighth Impedance Forum Paris, 1994, pp. 233–242.
[34] R. Rosset, D. Mercier, S. Douville, La mesure du pouvoir entartrant des eaux par des méthodes électrochimiques et les procédés antitartre (The measurement of scaling power of water by electrochemical methods and scale inhibitor processes), Annales des falsifications, de l'expertise chimique et toxicologique 90 (1997) 41–65.
[35] J. Ledion, B. François, J. Vienne, Caractérisation du pouvoir entartrant par précipitation contrôlée rapide (Characterization of scaling power controlled by rapid precipitation), J. Eur. Hydrol. 28 (1997) 15–35.
[36] H.S. Ras, S. Ghizellaoui, Influence of copper and zinc on the power furring of encrusting water, Energy Proc. 18 (2012) 1511–1522.
[37] L. Beaunier, C. Gabrielli, G. Poindessous, G. Maurin, R. Rosset, Investigation of electrochemical calcareous scaling, J. Electroanal. Chem. 501 (2001) 41–53.
[38] O. Devos, C. Gabrielli, B. Tribollet, Simultaneous EIS and *in situ* microscope observation on a partially blocked electrode application to scale electrodeposition, Electrochim. Acta 51 (2006) 1413–1422.
[39] G. Gauthier, Y. Chao, O. Horner, O. Alos-Ramos, F. Hui, J. Lédion, H. Perrot, Application of the fast controlled precipitation method to assess the scale-forming ability of raw river waters, Desalination 299 (2012) 89–95.
[40] S.H. Welling, F. Hubálek, J. Jacobsen, D.J. Brayden, U.L. Rahbek, S.T. Buckley, The role of citric acid in oral peptide and protein formulations: Relationship between calcium chelation and proteolysis inhibition, Eur. J. Pharm. Biopharm. 86 (2014) 544–551.
[41] M. Kakiage, K. Iwase, H. Bayashi, Effect of citric acid addition on disaggregation of crystalline hydroxyapatite nanoparticles under calcium-rich conditions, Mater. Lett. 156 (2015) 39–41.
[42] C.h. Barchiche, C. Deslouis, D. Festy, O. Gil, P.h. Refait, S. Touzain, B. Tribollet, Characterization of calcareous deposits in artificial sea water by impedance techniques 3-deposit of $CaCO_3$ in the presence of Mg(II), Electrochim. Acta 48 (2003) 1645–1654.
[43] N. Abdel-Aal, K. Sawada, Inhibition of adhesion and precipitation of $CaCO_3$ by aminopolyphosphonate, J. Cryst. Growth 256 (2003) 188–200.